PHYSICAL REVIEW B **86**, 024428 (2012)

Universality and critical behavior at the critical endpoint in the itinerant-electron metamagnet UCoAl

K. Karube,[1,*] T. Hattori,[1] S. Kitagawa,[1] K. Ishida,[1] N. Kimura,[2,3] and T. Komatsubara[2,3]
[1]*Department of Physics, Graduate School of Science, Kyoto University, Kyoto 606-8502, Japan*
[2]*Department of Physics, Graduate School of Science, Tohoku University, Sendai 980-8578, Japan*
[3]*Center for Low Temperature Science, Tohoku University, Sendai 980-8578, Japan*
(Received 25 April 2012; published 23 July 2012)

We performed nuclear-magnetic-resonance measurements on itinerant-electron metamagnet UCoAl to investigate the critical behavior of the magnetism near a metamagnetic (MM) critical endpoint (CEP). We derived c-axis magnetization M_c and its fluctuation S_c from the measurements of Knight shift and nuclear spin-lattice relaxation rate $1/T_1$ as a function of the c-axis external field (H_c) and temperature (T). We developed contour plots of M_c and S_c on the H_c-T phase diagram, and observed the strong divergence of S_c at the CEP. The critical exponents of M_c and S_c near the CEP are estimated and found to be close to the universal properties of a three-dimensional Ising model. We indicate that the critical phenomena at the itinerant-electron MM CEP in UCoAl have a common feature as a gas–liquid transition.

DOI: 10.1103/PhysRevB.86.024428 PACS number(s): 76.60.−k, 75.40.Gb, 71.27.+a

I. INTRODUCTION

Magnetic properties on U compounds have attracted much interest since novel phenomena such as a hidden order in URu_2Si_2 (Refs. 1,2) and superconducting ferromagnet in UGe_2 (Ref. 3), URhGe (Ref. 4), and UCoGe (Ref. 5) were reported. In this paper, we report magnetic properties on UCoAl possessing the hexagonal ZrNiAl-type structure shown in Fig. 1. UCoAl shows a characteristic first-order metamagnetic (MM) transition at low temperatures.[6,7] The ground state of UCoAl is paramagnetic (PM) with a strong Ising-like anisotropy (the easy axis is the c axis), and magnetization (M) along the c-axis M_c shows an abrupt jump with hysteresis below 10 K, when relatively small external magnetic fields between 0.7–1 T are applied along the c axis.[6,7] This is the first-order MM transition from the PM state to the ferromagnetic (FM) state, but it is noted that UCoAl is an itinerant-electron metamagnet originating from U-5f electrons. The induced FM moments ($\sim$0.3 μ_B) are much smaller than the effective moments ($\sim$1.8 μ_B) evaluated from the Curie-Weiss behavior above 40 K, and M_c becomes larger with applied fields even above the MM transition. This first-order MM transition in UCoAl terminates at a finite temperature critical end point (CEP), $(\mu_0 H_c,\ T)_{\mathrm{CEP}} \sim$ (1 T, 12 K) (Refs. 7–9), as shown schematically in Fig. 2(a). It was suggested that UCoAl at ambient pressure is a similar state as UGe_2 at $P \sim 2$ GPa since the presence of a similar CEP was reported on UGe_2 in the pressure region of $1.5 < P < 3$ GPa (Ref. 10). Above the CEP, the borderline of the first-order transition becomes blurred and the PM state continuously connects to the FM state as a crossover. This CEP reminds us of a gas–liquid transition [see Fig. 2(b)], where the order parameter and the tuning parameter are the density of molecules and pressure, respectively.[11] Therefore, an important and fundamental question is what kind of universality class is observed near the itinerant-electron MM CEP since its universality has not been reported so far and the change of the electronic structure was recently suggested in the field-induced FM state.[12,13]

We point out that a precise field-tuned NMR study on the itinerant metamagnet UCoAl is an ideal experiment for investigating the physical properties around the CEP since (i) the MM transition in UCoAl occurs at relatively smaller magnetic fields, (ii) magnetic fields (tuning parameter) can be controlled continuously and precisely, and (iii) magnetization (order parameter) and its dynamical fluctuations can be detected by NMR measurements microscopically. For the study of a first-order transition, microscopic measurements are crucial since they can discriminate between homogeneous and inhomogeneous (coexisting) states explicitly.

II. EXPERIMENT

We performed ^{27}Al-NMR measurements on a single-crystal UCoAl. A single-crystal UCoAl sample was synthesized by the Czochralski pulling method in a tetra-arc furnace, and was cut as a rectangular cubic shape with 1.5 (a axis) $\times$ 3.2 (b axis) $\times$ 1.7 (c axis) mm^3. This single-crystal UCoAl was used for angle-resolved ^{27}Al-NMR measurements to investigate H_c (magnetic field along the c axis) and temperature dependencies of Knight shift K and nuclear spin-lattice relaxation rate $1/T_1$, by controlling the angle θ between the c axis and the external field H in the ac plane. NMR measurements were carried out at two frequencies of 29.8 MHz [$\mu_0 H(^{27}K = 0) = 2.686$ T] and 49.1 MHz [$\mu_0 H(^{27}K = 0) = 4.426$ T]. The typical H swept ^{27}Al and ^{59}Co-NMR spectra obtained under H parallel to the a axis ($\theta = 90^\circ$) at 29.8 MHz is shown in Fig. 3. All NMR peaks are well identified as shown in Fig. 3. In the field along the a axis, there exist two inequivalent ^{27}Al sites, denoted as ^{27}Al($\phi = 0^\circ$) and ^{27}Al($\phi = \pm 120^\circ$), where ϕ is the angle between the direction of the external field and the electric field gradient (EFG) second principal axis in a basal plane. These two inequivalent ^{27}Al nuclei ($I = 5/2$) each provide four quadrupole satellites at different resonance fields as calculated by the following first-order perturbation formula for the $m \leftrightarrow (m-1)$ transition

$$\Delta\nu_{m\leftrightarrow m-1} = \frac{\nu_{zz}}{2}\left(m - \frac{1}{2}\right)\{(3\cos^2\theta - 1) - \eta\sin^2\theta\cos 2\phi\}, \quad (1)$$

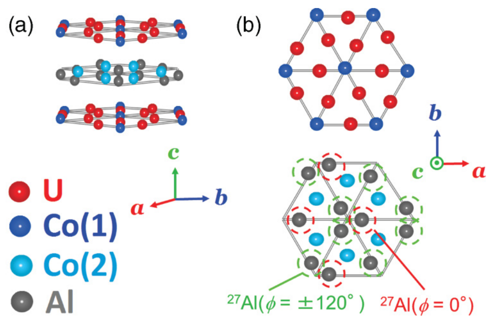

FIG. 1. (Color online) (a) Hexagonal crystal structure of UCoAl composed by the U-Co(1) layer and Co(2)-Al layer alternatively stacking along the c axis. (b) U-Co(1) layer and Co(2)-Al layer from the view of the c axis. When the external field is applied along the a axis, there exist two inequivalent Al sites, marked by a red circle for ^{27}Al($\phi = 0^\circ$) and a light green circle for ^{27}Al($\phi = \pm 120^\circ$), where ϕ is the angle between the direction of the external field and the EFG second principal axis in the basal plane.

where ν_{zz} is a quadrupole resonance frequency along the EFG principle axis (c axis), and η, defined as $|\nu_{xx} - \nu_{yy}|/\nu_{zz}$, is an asymmetry parameter about the EFG principal axis. From the observed ^{27}Al-NMR spectra and the above theoretical equation we obtained the quadrupole parameters for the ^{27}Al nucleus as shown in Table I. The quadrupole parameters of two Co sites in UCoAl are also listed in Table I.[14]

K and $1/T_1$ were measured at a central peak of ^{27}Al-NMR spectra, corresponding to the transition between the nuclear spin states $I = 1/2$ and $-1/2$. For the measurements of $1/T_1$, nuclear magnetization after saturation pulses can be fitted consistently with the theoretical function in whole measurements. The angle θ was controlled by using a split-coil superconducting magnet and a rotator with the precision of 0.5°.

III. EXPERIMENTAL RESULTS AND DISCUSSION

A. Ising-type anisotropy in magnetization and ferromagnetic fluctuations

NMR Knight shift, which is proportional to microscopic spin susceptibility at the nuclear site, and nuclear spin-lattice relaxation rate $1/T_1$, probing the electronic spin dynamics, are measured down to 1.5 K and in the magnetic field (H) up to 4.4 T. The upper panel of Fig. 4 shows T dependencies of the K in $\mu_0 H \sim 4.4$ T along the a and c axes. The Ising-type strong anisotropy $K_a \ll K_c$ was observed. The Knight shift $K(\theta)$ at the angle θ between an external field and the c axis is expressed as the relation of $K(\theta) = K_c \cos^2\theta + K_a \sin^2\theta$.

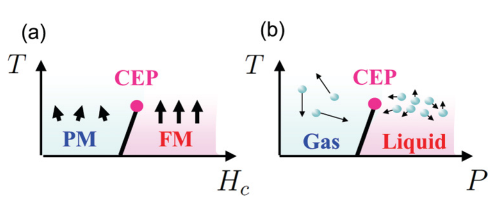

FIG. 2. (Color online) Schematic figures of (a) a MM transition and (b) a gas–liquid transition. Both figures have a CEP at a finite temperature. Below the CEP two phases are separated by the first-order transition line.

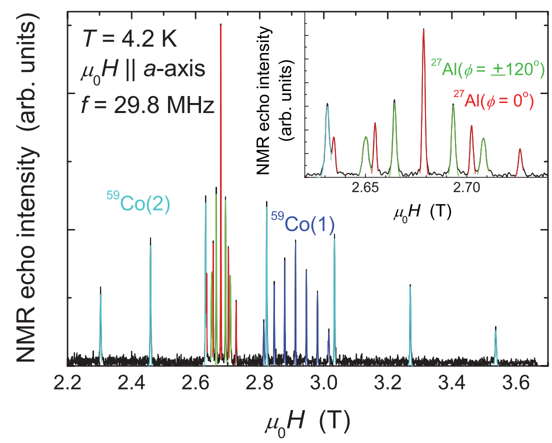

FIG. 3. (Color online) Field-swept NMR spectra at $T = 4.2$ K in the field applied along the a axis. The ^{59}Co-NMR spectra are shown with dark and light blue for ^{59}Co(1) and ^{59}Co(2) sites, and ^{27}Al-NMR spectra, which split into two sites in the H parallel to the a axis, are shown with red and green for ^{27}Al($\phi = 0^\circ$) and ^{27}Al($\phi = \pm 120^\circ$), respectively. Here, ϕ is the angle between the direction of the external field and the EFG second principal axis in a basal plane.

Using this relation, the c-axis magnetization at the ^{27}Al nucleus site was evaluated as

$$M_c' = K_c \mu_0 H_c = \mu_0 H_c [K(\theta) - K_a \sin^2\theta] \cos^{-2}\theta. \quad (2)$$

Here we labeled M_c' instead of M_c to make clear that this magnetization calculated from the Knight shift contains the demagnetization effect. Now we need to estimate the M_c without the demagnetization effect. The shape of the sample in the applied field is almost the same rectangle (ac plane vs b axis, the ratio of the length is $b/a(c) \sim 2$). Thus, the demagnetization field in units of μ_B is estimated as $D = 0.064\ \mathrm{T}/\mu_B$. Using the hyperfine-coupling constant A_{hf} between the ^{27}Al nucleus and U-5f electron, the demagnetization factor D and bulk magnetization M_c^{bulk} from the U-5f moment along the c axis without the demagnetization effect, M_c' is written as follows:

$$M_c' = A_{\mathrm{hf}} M_c^{\mathrm{bulk}} - D M_c^{\mathrm{bulk}} \equiv A_{\mathrm{hf}}' M_c^{\mathrm{bulk}}. \quad (3)$$

Here we define the hyperfine-coupling constant with demagnetization as $A_{\mathrm{hf}}' \equiv A_{\mathrm{hf}} - D$. A_{hf}' is estimated as $0.80\ \mathrm{T}/\mu_B$ from $K_c \mu_0 H_c$ vs M_c^{bulk} plot. Thus, M_c without demagnetization is corrected as follows:

$$M_c = A_{\mathrm{hf}} M_c^{\mathrm{bulk}} = (1 + D/A_{\mathrm{hf}}') M_c' \sim 1.08 M_c'. \quad (4)$$

The lower panel of Fig. 4 shows the T dependence of the calculated M_c, in which M_c^{bulk} measured in the field $\mu_0 H = 4.0$ T is also plotted.[8] The calculated M_c is well scaled to M_c^{bulk} with the hyperfine-coupling constant $A_{\mathrm{hf}} = 0.86\ \mathrm{T}/\mu_B$. This

TABLE I. NQR parameters of ^{59}Co(1), ^{59}Co(2), and ^{27}Al nuclei in UCoAl.

Nucleus	ν_{zz} (MHz)	η	Reference
^{59}Co(1)	0.695	0	Iwamoto et al. (Ref. 14)
^{59}Co(2)	4.32	0	Iwamoto et al. (Ref. 14)
^{27}Al	0.385	0.327	This work

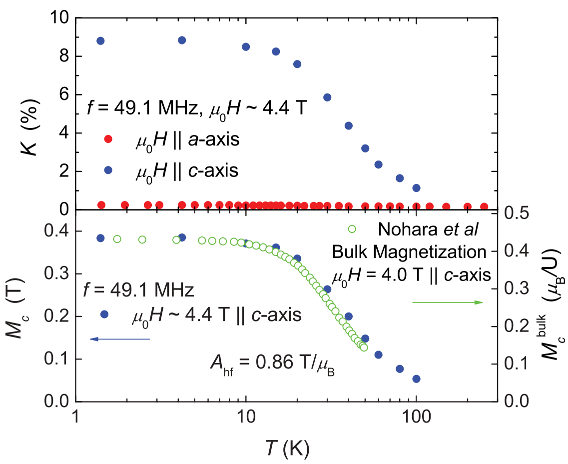

FIG. 4. (Color online) (Upper panel) Temperature dependence of Knight shift K in the field $\mu_0 H \sim 4.4$ T applied along the a axis (red circle) and the c axis (blue circle). (Lower panel) Temperature dependence of magnetization along the c-axis M_c evaluated with the above ^{27}Al-NMR Knight-shift results (blue circle) and bulk magnetization along the c axis ($M_c^{\rm bulk}$) in $\mu_0 H_c = 4.0$ T (green open circle) (Ref. 8). M_c and $M_c^{\rm bulk}$ were well scaled with the hyperfine-coupling constant $A_{\rm hf} = 0.86$ T/$\mu_{\rm B}$.

verifies that ^{27}Al-NMR results are determined by the U-5f magnetic properties.

The upper panel of Fig. 5 shows the T dependence of $(T_1T)^{-1}$ in the field ($\mu_0 H \sim 4.4$ T) along the a and c axes, respectively. In contrast with the Knight-shift behavior, $(T_1T)^{-1}$ along the a axis $[(T_1T)_a^{-1}]$ shows temperature dependence with a broad maximum around 20 K and the Korringa relation (T_1T = const.) below 7 K, but $(T_1T)^{-1}$ along the c axis $[(T_1T)_c^{-1}]$ is nearly constant with a small value. This is because $(T_1T)^{-1}$ probes hyperfine-field fluctuations perpendicular to the applied fields. Thus, $(T_1T)^{-1}$ measured in

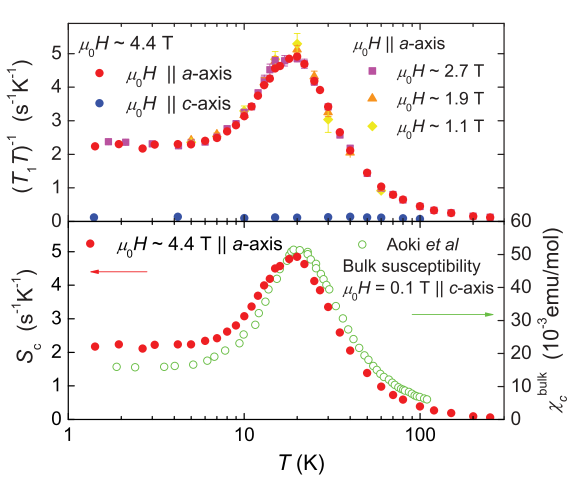

FIG. 5. (Color online) (Upper panel) Temperature dependence of $(T_1T)^{-1}$ in the field $\mu_0 H \sim 4.4$ T applied along the a axis (red circle) and c axis (blue circle). $(T_1T)^{-1}$ in the different fields along the a axis are also plotted. (Lower panel) Temperature dependence of magnetic fluctuation S_c along the c axis evaluated with above $(T_1T)^{-1}$ results, together with bulk magnetic susceptibility $\chi_c^{\rm bulk}$ in $\mu_0 H \sim 0.1$ T along the c axis (green open symbol) (Ref. 9). S_c and $\chi_c^{\rm bulk}$ are well scaled with each other.

a field along the i direction is expressed as $(T_1T)_i^{-1} \equiv S_j + S_k$, where $S_{j,(k)}$ are magnetic fluctuations along the $j,(k)$ direction $[S_{j,(k)} \propto \sum_q |S_{j,(k)}(q,\omega \sim 0)|]$ and i, j, and k directions are mutually orthogonal. In addition, $(T_1T)^{-1}$ at the angle θ is expressed as, $(T_1T)^{-1}(\theta) = (T_1T)_c^{-1}\cos^2\theta + (T_1T)_a^{-1}\sin^2\theta$. If we assume that the in-plane magnetic fluctuations are isotropic $[(T_1T)_c^{-1} \equiv S_a + S_b \sim 2S_a]$, S_c is evaluated as

$$S_c = \left[(T_1T)^{-1}(\theta) - \frac{(1+\cos^2\theta)(T_1T)_c^{-1}}{2}\right]\sin^{-2}\theta \qquad (5)$$

from the measurements of $(T_1T)_c^{-1}$ and $(T_1T)^{-1}(\theta)$. The lower panel of Fig. 5 shows the T dependence of S_c calculated with Eq. (5) by using the upper-panel $(T_1T)^{-1}$ data. In the figure, the T dependence of bulk magnetic susceptibility $\chi_c^{\rm bulk}$ measured in the field $\mu_0 H = 0.1$ T along the c axis was also plotted.[9] The good scaling between S_c and $\chi_c^{\rm bulk}$ indicates that the magnetic fluctuations along the c axis are completely insensitive to the field along the a axis and suggests that the magnetic fluctuations originating from the U-5f electrons possess the three-dimensional (3-D) FM fluctuations since the relation of $[(T_1T)^{-1} \propto \chi]$ was anticipated in the self-consistent-renormalization (SCR) theory when 3-D FM fluctuations are dominant.[15] The presence of the 3-D FM fluctuations is also consistent with the resistivity data $[\rho(T) \propto T^{5/3}]$ measured in zero field.[18] We comment that the similar Ising magnetic fluctuations were observed in a FM superconductor UCoGe (Refs. 16,17).

B. H_c dependence of M_c and S_c

To investigate the dependence of M_c and S_c against magnetic fields along the c axis (H_c), we measured $K(\theta)$ and $(T_1T)^{-1}(\theta)$ by controlling the angle θ in the ac plane [the c axis ($\theta = 0^\circ$) and the a axis ($\theta = 90^\circ$)]. This is because the applied magnetic field is decomposed to the fields along the a axis (H_a) and c axis (H_c) with respect to the sample, and M_c and S_c are not affected by H_a, but very sensitive to H_c. This experimental condition enabled us to control $H_c (= H\cos\theta)$ continuously with a fixed NMR frequency $f_0 = 49.1$ MHz, and thus to scan H_c across the CEP. Figures 6 and 7 show T variation of the ^{27}Al-NMR spectra below and above the critical field of $\mu_0 H_c \sim 1$ T, respectively. NMR spectra obtained below $\mu_0 H_c \sim 1$ T (Fig. 6) show a discontinuous shift around 10 K with a coexistence of the PM and FM spectra. The field difference between the PM and FM signals is much larger than the demagnetization field ($-DM_c^{\rm bulk} \sim -0.02$ T), and the demagnetization field works to reduce the field difference between the two signals. Therefore, we consider that the coexistence of the PM and FM signals is not due to the demagnetization effect, but due to the first-order transition. On the other hand, NMR spectra obtained above $\mu_0 H_c \sim 1$ T (Fig. 7) show a continuous shift with decreasing temperature. The NMR measurements is a powerful technique to distinguish between the first-order transition and crossover in MM behavior.

Figure 8 shows the H_c dependence of M_c (upper panel) and S_c (lower panel) at several fixed temperatures. At $T = 4.2$ and 10 K, M_c shows a first-order transition from the PM to FM state with a coexisting region where NMR signals from

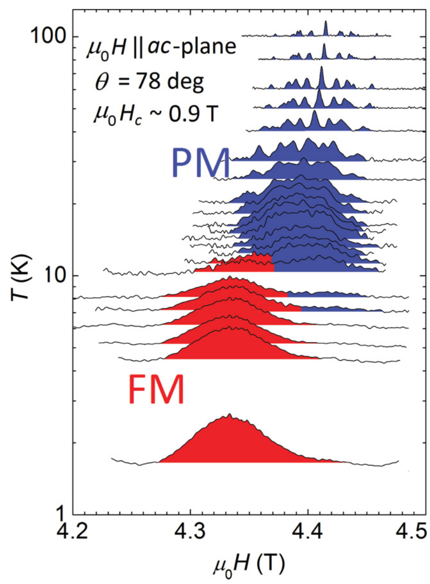

FIG. 6. (Color online) Temperature scanned [27]Al-NMR spectra at the angle $\theta = 78^\circ$ ($\mu_0 H_c \sim 0.9$ T) in the first-order transition region. [27]Al-NMR spectra colored by blue and red represent PM and FM components, respectively. Between 11 and 7 K both of the PM and FM signals appear, where the PM and FM components coexist.

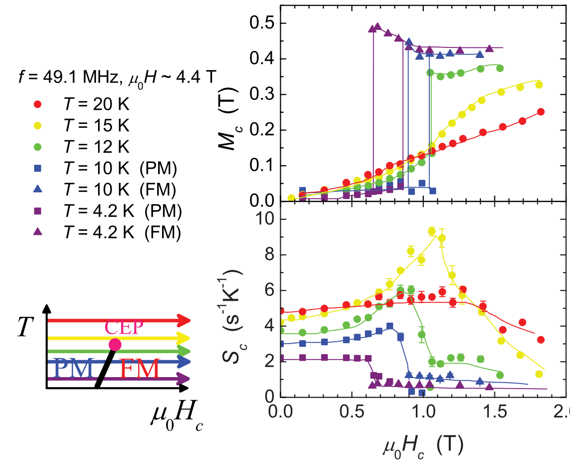

FIG. 8. (Color online) H_c dependence of M_c and S_c at several fixed temperatures. At 4.2 and 10 K, PM and FM components separated by the first-order transition are denoted as square and triangle symbols, respectively. At the other temperatures, data points are denoted as circle symbols. The measurement scans are shown in the schematic H_c-T phase diagram by colored arrows. Each color of an arrow corresponds to that of data points.

the PM and FM states were observed. Above $T = 12$ K, the first-order transition disappears and M_c continuously changes against H_c. Correspondingly, S_c at 4.2 and 10 K suddenly drops at the MM transition field without a notable divergence, but S_c of the PM component also drops to the same value as that of the FM component. At 12 and 15 K, very close to a critical temperature, S_c exhibits a pronounced peak around $\mu_0 H_c \sim 1$ T, and the peak becomes suppressed by getting away from the critical temperature.

Figure 9 shows the T dependence of M_c (upper panel) and S_c (lower panel) at fixed several angles θ (i.e., $H_c = H\cos\theta$). In the PM region, M_c shows the broad maximum around 20 K, defined as $T_{\max}$. $T_{\max}$ slightly decreases with increasing H_c. In a region between $\mu_0 H_c \sim 0.7$ and 1.0 T, NMR signals from the PM and FM states were observed as shown in Fig. 6, indicative of the phase separation driven by the first-order transition as observed in the H_c scanned measurements. Above $\mu_0 H_c \sim 1.0$ T, the first-order transition disappears and changes to a crossover as shown in Fig. 7. At the PM region, S_c shows almost the same peak structure as M_c. It should be noted that this peak was observed even at $\mu_0 H_c = 0$ T, suggesting that the novel longitudinal magnetic fluctuations are present in zero field. This unstable ground state with strong longitudinal

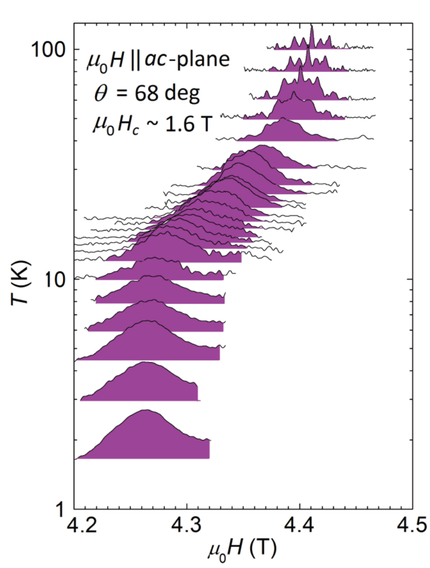

FIG. 7. (Color online) Temperature scanned [27]Al-NMR spectra at the angle $\theta = 68^\circ$ ($\mu_0 H_c \sim 1.6$ T) in the crossover region. [27]Al-NMR spectra colored purple continuously shift.

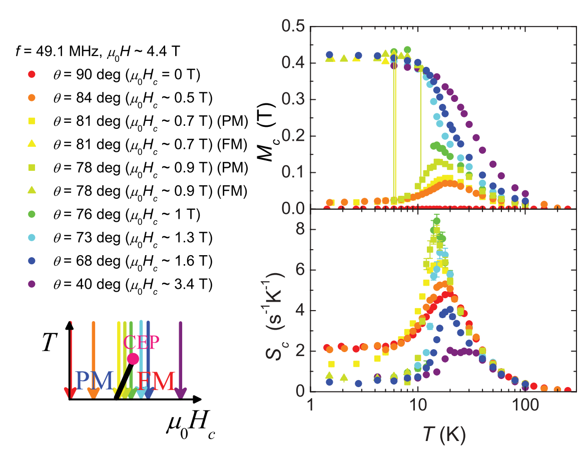

FIG. 9. (Color online) Temperature dependence of M_c and S_c for several fixed θ (i.e., H_c). At $\mu_0 H_c = 0.7$ and 0.9 T, the PM and FM components separated by the first-order transition are denoted as square and triangle symbols, respectively. At other H_c, data points are denoted as circle symbols. The measurement scans are shown in the schematic H_c-T phase diagram by colored arrows. Each color of an arrow corresponds to that of data points.

FM fluctuations leads UCoAl to the MM transition in a very small external field. In fact, Yamada *et al*. reported that the MM transition and susceptibility-maximum phenomena are explained with the phenomenological spin-fluctuation model for itinerant-electron metamagnetism.[19,20] With increasing H_c, the peak of S_c slightly shifts to lower temperatures and its intensity grows. When the H_c exceeds the first-order transition field, the peak of S_c rapidly falls down in the FM region. It is also noteworthy that S_c of the PM and FM components possesses almost the same values, although M_c of the PM and FM is different in the phase-separation region as observed in the above H_c scanned measurements. These are quite unusual since the S_c of the two states is different in most phase-separation (first-order) phenomena.[21] We suggest that anomalous phase-separation might occur, where the magnetic state is fluctuating between the PM and FM states. Magnetic properties in the coexisting region thus deserve further investigations.

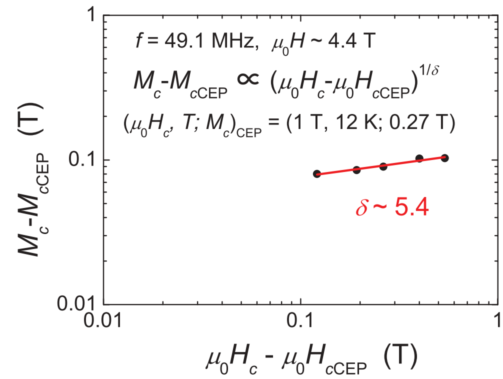

FIG. 11. (Color online) The power-law fitting of M_c vs H_c on logarithmic scales, where the CEP determined as $(\mu_0 H_c, T; M_c)_{\rm CEP} =$ (1 T, 12 K; 0.27 T). The fitting provided the critical exponent as $\delta \sim 5.4$.

C. Contour plots of M_c and S_c

Based on the H_c and T scanned measurements of M_c and S_c, we developed the contour plots of M_c and S_c in the H_c-T plane, which are shown in Figs. 10(a) and (b), respectively. In the figures, the red (blue) circles show the points where the FM (PM) NMR signal appears (disappears) with increasing H_c or decreasing T, and thus the gray-colored region surrounded by these symbols indicates the coexistence of the PM and FM components. The light green triangle symbol denotes the point where M_c shows the maximum against T in the PM region. The crossover points determined with a maximum of $\partial M_c/\partial T$ are denoted as yellow squares, and the CEP is marked as a star point. It is shown that M_c changes continuously from the PM to FM state if the system is varied by following the arrow around the CEP although the transition from the PM and FM states is a first-order transition in small fields. Furthermore, S_c diverges significantly at the CEP and gradually decays in the crossover region. The divergence of S_c was also suggested by the measurement of the nuclear spin-spin relaxation rate $1/T_2$ in the ^{59}Co-NMR (Refs. 8,22). These are well known phenomena observed at a gas–liquid transition. In contrast, M_c and S_c show a broad maximum around 20 K in the low-field PM state, which originates from the specific structure of the density of states near the Fermi energy $E_{\rm F}$, and the maximum merges with the CEP with increasing H_c. The peak structure of M_c and S_c in the PM region is a characteristic feature of itinerant-electron metamagnets, but has not been observed in a gas–liquid transition.

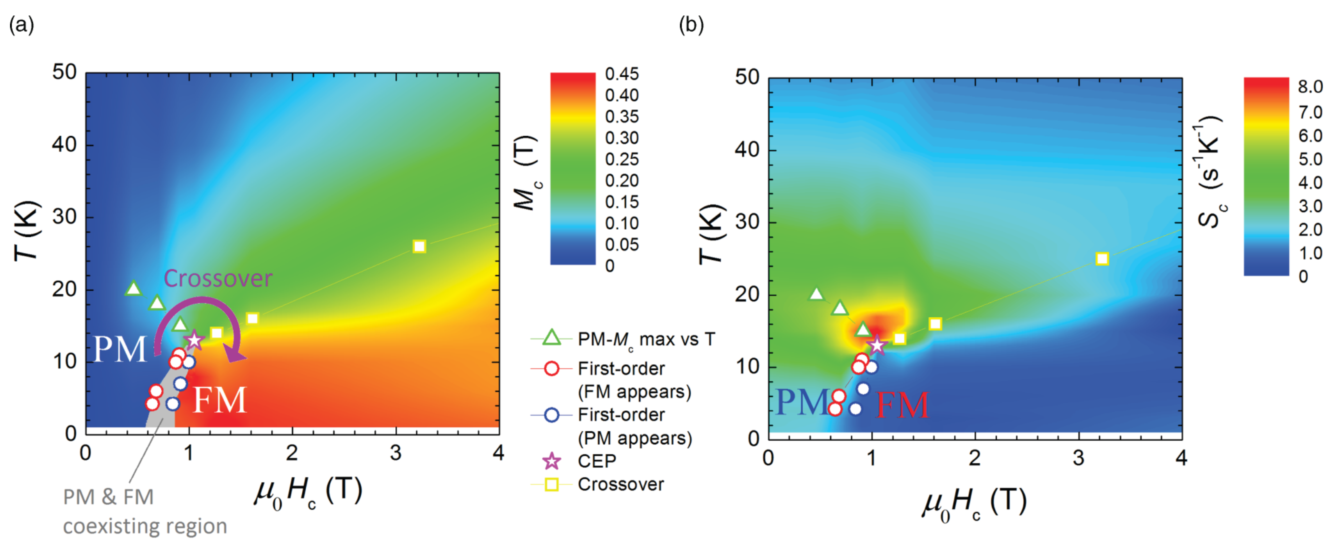

FIG. 10. (Color online) (a) Magnetization along the c axis M_c in UCoAl is shown by a contour plot in the H_c-T phase diagram. In the phase diagram, the red (blue) circle symbol denotes the point where the FM component starts to appear (disappear) by the first-order transition between the PM to FM state. The surrounded area by the red and blue circle symbols (gray colored region) shows the region where the PM and FM components coexist. The light green triangle symbol denotes the point of the temperature $T_{\rm max}$ where M_c has a broad maximum in the PM region. The yellow square symbol denotes the point of crossover determined from the maximum of $\partial M_c/\partial T$. The star symbol denotes the CEP determined as $(\mu_0 H_c, T)_{\rm CEP} \sim$ (1 T, 12 K). Passing outside the CEP along the purple arrow, M_c changes continuously from the PM to FM states. (b) Magnetic fluctuation along the c axis S_c in UCoAl is shown by contour plot in the H_c-T phase diagram.

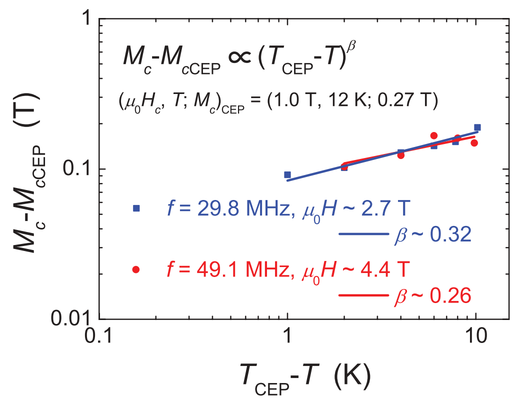

FIG. 12. (Color online) The power-law fitting of M_c vs T on logarithmic scales, where the CEP determined as $(\mu_0 H_c, T; M_c)_{\rm CEP} =$ (1 T, 12 K; 0.27 T). The fitting provided the critical exponent as $\beta \sim$ 0.26. Two cases of f = 29.8 MHz ($\mu_0 H \sim 2.7$ T) and f = 49.1 MHz ($\mu_0 H \sim 4.4$ T) provided the almost same fitting result.

D. Critical phenomena around CEP

In general, the critical phenomena close to the CEP has been analyzed on the basis of "critical exponents." In the estimation of the critical exponents, we set the CEP as $(\mu_0 H_c, T; M_c)_{\rm CEP}$ = (1 T, 12 K; 0.27 T). In addition, we used low-energy dynamical susceptibility S_c for the γ estimation, except for data points close to the CEP. This is because the divergence of the susceptibility is sensitively affected by the ambiguities in the determination of H_c and misalignment of the sample, but the value of γ would be reliable if a wide temperature range is taken for the estimation. The critical exponents were estimated as $(\delta, \beta, \gamma) \sim (5.4, 0.26, 1.2)$ from the fitting shown in Figs. 11, 12, and 13. Note that these results almost satisfy the scaling relation $\gamma \sim \beta(\delta - 1)$ indicating that the values are evaluated reasonably. The critical exponents (δ, β, γ) are plotted along with those of the known universality classes in Fig. 14. We found that the universality class observed around the CEP in UCoAl is close to the 3-D critical classes (3-D Ising, 3-D XY, and 3-D Heisenberg). However, since UCoAl possesses the strong Ising anisotropy in the static and dynamic magnetic properties, it is reasonable to conclude that UCoAl exhibits a 3-D Ising one, which is the same universality class as a gas–liquid

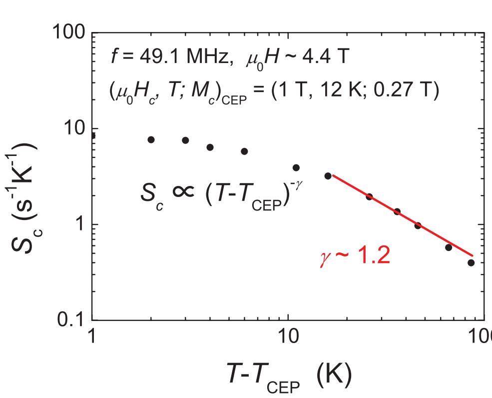

FIG. 13. (Color online) The power-law fitting of S_c vs T on logarithmic scales, where the CEP determined as $(\mu_0 H_c, T; M_c)_{\rm CEP} =$ (1 T, 12 K; 0.27 T). The fitting provided the critical exponent as $\gamma \sim 1.2$.

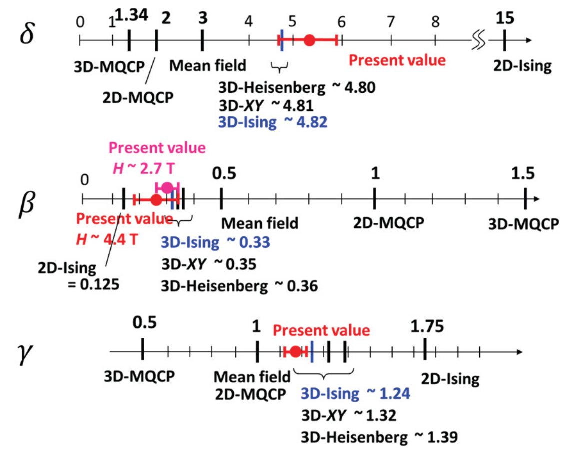

FIG. 14. (Color online) Comparison of the critical exponents (δ, β, γ) of the present case with those of the known universality classes [mean-field, 2-D Ising, 3-D Ising, 3-D XY, 3-D Heisenberg, 2-D marginal quantum critical point (2-D MQCP) and 3-D marginal quantum critical point (3-D MQCP) model].

transition. The similar universality class was reported in the critical behavior of the conductivity near the 3-D Mott system of Cr-doped V_2O_3 (Ref. 24). In contrast, an unconventional critical behavior was reported at the Mott transition occurring in a quasi-two-dimensional (2-D) organic conductor, probably due to the low dimensionality of the system.[23] Therefore, the critical behavior at the finite-temperature MM CEP occurring in UCoAl is a textbook example of the 3-D Ising universality, but the critical behavior when the CEP is tuned to zero temperature [the so-called quantum critical end point (QCEP)] deserve to be investigated since an unconventional universality featured by the topological transition of Fermi surfaces was suggested at the QCEP.[13]

IV. CONCLUSION

We derived c-axis magnetization M_c and its fluctuation S_c as a function of H_c and T from ^{27}Al-NMR measurements for single-crystal UCoAl. The NMR measurements revealed that UCoAl possesses the 3-D FM fluctuations with the strong Ising-type anisotropy. Based on the H_c and T scanned measurements, the contour plot of M_c and S_c are developed, and the divergence of S_c, which is an anticipated behavior at the CEP, is shown. The critical exponents near the CEP of the itinerant MM transition are evaluated, and are found to be categorized to the 3-D Ising universality, which is the same universality class observed in gas–liquid and 3-D Mott transitions.

ACKNOWLEDGMENTS

The authors thank H. Ikeda, H. Kotegawa, H. Nohara, H. Kitamura, K. Matsuda, and M. Yao for valuable discussions, and T. Asai, Y. Ihara, Y. Nakai, S. Yonezawa, and Y. Maeno for experimental support and valuable discussions. This work was partially supported by Kyoto University LTM Centre; the "Heavy Electrons" Grant-in-Aid for Scientific Research on Innovative Areas (No. 20102006) from the Ministry of

Education, Culture, Sports, Science, and Technology (MEXT) of Japan; a Grant-in-Aid for the Global COE Program "The Next Generation of Physics, Spun from Universality and Emergence" from MEXT of Japan; and a Grant-in-Aid for Scientific Research from the Japan Society for Promotion of Science (JSPS).

---

*karube@scphys.kyoto-u.ac.jp

[1] T. T. M. Palstra, A. A. Menovsky, J. van den Berg, A. J. Dirkmaat, P. H. Kes, G. J. Nieuwenhuys, and J. A. Mydosh, Phys. Rev. Lett. **55**, 2727 (1985).

[2] M. B. Maple, J. W. Chen, Y. Dalichaouch, T. Kohara, C. Rossel, and M. S. Torikachvili, M. W. McElfresh, and J. D. Thompson, Phys. Rev. Lett. **56**, 185 (1986).

[3] S. S. Saxena, P. Agarwal, K. Ahilan, F. M. Grosche, R. K. W. Haselwimmer, M. J. Steiner, E. Pugh, I. R. Walker, S. R. Julian, P. Monthoux, G. G. Lonzarich, A. Huxley, I. Sheikin, D. Braithwaite, and J. Flouquet, Nature (London) **406**, 587 (2000).

[4] D. Aoki, A. Huxley, E. Ressouche, D. Braithwaite, J. Flouquet, J.-P. Brison, E. Lhotel, and C. Paulsen, Nature (London) **413**, 613 (2001).

[5] N. T. Huy, A. Gasparini, D. E. de Nijs, Y. Huang, J. C. P. Klaasse, T. Gortenmulder, A. de Visser, A. Hamann, T. Görlach, and H. V. Löhneysen, Phys. Rev. Lett. **99**, 067006 (2007).

[6] A. V. Andreev, R. Z. Levitin, Yu. F. Popov, and R. Yu. Yumaguzhin, Sov. Phys. Solid State **27**, 1145 (1985).

[7] N. V. Mushnikov, T. Goto, K. Kamishima, H. Yamada, A. V. Andreev, Y. Shiokawa, A. Iwao, and V. Sechovsky, Phys. Rev. B **59**, 6877 (1999).

[8] H. Nohara, H. Kotegawa, H. Tou, T. D. Matsuda, E. Yamamoto, Y. Haga, Z. Fisk, Y. Onuki, D. Aoki, and J. Flouquet, J. Phys. Soc. Jpn. **80**, 093707 (2011).

[9] D. Aoki, T. Combier, V. Taufour, T. D. Matsuda, G. Knebel, H. Kotegawa, and J. Flouquet, J. Phys. Soc. Jpn. **80**, 094711 (2011).

[10] V. Taufour, D. Aoki, G. Knebel, and J. Flouquet, Phys. Rev. Lett. **105**, 217201 (2010).

[11] L. Kadanoff, W. Gotze, D. Hamblem, R. Hecht, E. A. S. Lewis, V. V. Palciauskas, M. Rayl, and J. Swift, Rev. Mod. Phys. **39**, 395 (1967).

[12] T. D. Matsuda, H. Sugawara, Y. Aoki, H. Sato, A. V. Andreev, Y. Shiokawa, V. Sechovsky, and L Havela, Phys. Rev. B **62**, 13852 (2000).

[13] Y. Yamaji, T. Misawa, and M. Imada, J. Phys. Soc. Jpn. **76**, 063702 (2007).

[14] Y. Iwamoto, K. Ueda, T. Kohara, A. V. Andreev, L. Havela, and V. Sechovsky, J. Magn. Magn. Mater. **234**, 207 (2001).

[15] T. Moriya and K. Ueda, Solid State Commun. **15**, 169 (1974).

[16] Y. Ihara, T. Hattori, K. Ishida, Y. Nakai, E. Osaki, K. Deguchi, N. K. Sato, and I. Satoh, Phys. Rev. Lett. **105**, 206403 (2010).

[17] T. Hattori, Y. Ihara, Y. Nakai, K. Ishida, Y. Tada, S. Fujimoto, N. Kawakami, E. Osaki, K. Deguchi, N. K. Sato, and I. Satoh, Phys. Rev. Lett. **108**, 066403 (2012).

[18] L. Havela, A. Kolomiets, F. Honda, A. V. Andreev, V. Sechovsky, L. E. DeLong, Y. Shiokawa, T. Kagayama, and G. Oomi, Physica B **281**, 379 (2000); **282**, 379 (2000).

[19] H. Yamada, Phys. Rev. B **47**, 11211 (1993).

[20] H. Yamada, N. V. Mushnikov, and T. Goto, J. Phys. Chem. Solid. **63**, 1189 (2002).

[21] T. Koyama, M. Nakamura, T. Mito, S. Wada, and J. L. Sarrao, Phys. Rev. B **71**, 184437 (2005).

[22] Quite recently, Nohara *et al.* (Ref. 8) reported that the nuclear spin-spin relaxation rate $1/T_2$ diverges remarkably at the CEP, but the divergence remains up to fields higher than 5 T, where the MM transition anomaly disappears. The present $1/T_1$ result is different from their $1/T_2$ results, and we consider that the former is more reliable than the latter since $1/T_2$ is easily affected by interactions other than electronic spin dynamics, such as static susceptibility and the interactions between nuclear spins.

[23] F. Kagawa, K. Miyagawa, and K. Kanoda, Nature (London) **436**, 534 (2005).

[24] P. Limelette, A. Georges, D. Jerome, P. Wzietek, P. Metcalf, and J. M. Honig, Science **302**, 89 (2003).